

A Validated Method for Titanium Implant Anchorage Analysis using MicroCT and Biomechanical Testing

Gabet Y^{1*} and Bab I²

¹Bone Research Laboratory, Sackler Faculty of Medicine, Tel Aviv University, Tel Aviv, Israel

²Bone Laboratory, Institute of Dental Sciences, Faculty of Dental Medicine, The Hebrew University of Jerusalem, Jerusalem, Israel

Abstract

We present here a protocol for the combined microstructural and biomechanical evaluation of endosseous titanium implant anchorage. The protocol is highly relevant for orthopedic and oral surgery experimentalists studying endosseous implantation, a discipline comprising ~ 150 publications yearly. The protocol is based on (i) insertion of titanium mini-implants horizontally into the rat proximal tibial metaphysis; (ii) quantitative microstructural evaluation by micro-computed tomography, including assessment of the bone-implant contact; (iii) correction of the bias due to implant positioning; (iv) biomechanical pullout testing using a customized jig for linear axial loading. A highlight of the protocol is image guided failure assessment consisting of time-lapsed biomechanical-microstructural analysis of the peri-implant bone deformation during implant pullout. Using this protocol we have demonstrated highly significant correlations between key microstructural and mechanical parameters. More importantly, we showed how changes to the metabolic state of the organism, like gonadectomy and bone anabolic agents, as well as implant surface properties affect the distribution and magnitude of critical strains in the peri-implant bone.

Keywords: Implants; Osteoporosis; Trabecular bone; Computed tomography; Biomechanics

Introduction

The use of uncemented titanium endosseous implants for restorative dentistry and orthopaedic surgery has been the standard of care for several decades. Endosseous implantation using uncemented titanium prostheses is commonly performed in trabecular bone sites such as the jaws, vertebrae and ileum. Still, the mechanisms involved in this fascinating and unique interaction between a living tissue and foreign substance are poorly understood. An important reason for the absence of sufficient mechanistic information is the lack of robust experimental models combined with solid tools to analyze structure-function relationships of the implant-bone system. Qualitative and quantitative *ex vivo* analysis of peri-implant tissues is typically done by means of light microscopy using thin histological sections following implant removal or thicker ground sections which contain the implant and undecalcified bone [1,2]. These techniques are labor-intensive and thus time-consuming. Moreover, they allow tissue quantification in only a limited number of two-dimensional images, and therefore exhibit inherent deficits in representativeness and/or accuracy. Furthermore, since all of these techniques are destructive, the specimens could not be further subjected to biomechanical testing, precluding correlative analyses to decipher the underlying causative microstructural changes. By contrast, micro-computed tomography (μ CT) is nondestructive, relatively fast and produces full, high-resolution three-dimensional (3-D) images of the implant and surrounding bone. Over the last 15 years, high-resolution micro-CT has set new gold-standards for the morphometric analysis of bone microarchitecture. Expectedly, this technology is also increasingly used in the experimental evaluation of endosseous implants. It does not require any specimen preparation and facilitates relatively rapid quantification based on three-dimensional (3D) reconstruction of the entire specimen rather than a limited number of planes typically sampled using 2D methods. The reliability of this technology in assessing 360° PIB is now well-established. It does not expose the specimen to any destructive procedures, a feature enabling combined microstructural-biomechanical evaluation thus

attaining unrivaled insights into structure-function relationships of the bone-implant system.

Despite these clear advantages, the implementation of μ CT in implant research remains limited. While these reports demonstrate the feasibility of using μ CT for studying the anchorage of endosseous implants, some major technical issues still await a solution before this technology becomes the state-of-art in implant biology.

One prerequisite for the successful anchorage of endosseous implants is *de novo* bone formation that leads to osseointegration (OI, direct bone-implant contact). A second critical factor for mechanical fixation is the peri-implant bone (PIB) mass which connects the implant to the external cortical envelope [3,4].

Major hurdles to overcome are (i) the X-ray scattering artifacts, which do not allow the use of standard gray value segmentation of the bone, implant and bone-marrow at the 100-200 μ m layer closest to the implant, thus disabling a quantitative measurement of the BIC. This consideration has a critical impact on the protocol design in terms of the implantation model, specimen orientation relative to the X-ray beam and the micro-CT operating settings. More importantly, because optimization based on these considerations failed to completely eliminate the artifact, we have further removed the scattering by applying multiple threshold values inversely related to the distance from the implant; (ii) non-standard implant positioning, which is corrected using a custom algorithm or by eliminating specimens positioned away from a predetermined location.

*Corresponding author: Yankel Gabet, Tel Aviv University, P.O. Box 39040, Tel Aviv 69978, Israel, Tel: 97236407684; Fax: 972-3-6407628; E-mail: yankel@tau.ac.il

Received June 02, 2016; Accepted June 06, 2016; Published June 13, 2016

Citation: Gabet Y, Bab I (2016) A Validated Method for Titanium Implant Anchorage Analysis using MicroCT and Biomechanical Testing. Adv Tech Biol Med 4: 180. doi: [10.4172/2379-1764.1000180](http://dx.doi.org/10.4172/2379-1764.1000180)

Copyright: © 2016 Gabet Y, et al. This is an open-access article distributed under the terms of the Creative Commons Attribution License, which permits unrestricted use, distribution, and reproduction in any medium, provided the original author and source are credited.

In the present study we report a rat model that combines implantation of titanium screw into a skeletal site that consists of both cortical and trabecular bone, with μ CT analysis of OI and PIB parameters and biomechanical testing.

Using this model, we were able to demonstrate the temporal pattern of OI formation and PIB remodeling, to establish a significant correlation between the percent implant surface in contact with bone (%OI) and biomechanical parameters and to discriminate between the osseous responses to different implant surface textures.

Materials and Methods

Animals

The experimental protocol was approved by the Institutional Animal Care and Use Committee of the Hebrew University-Hadassah Medical Center. Thirteen-week old male Sprague-Dawley rats were purchased from Harlan Laboratories (Jerusalem, Israel) and maintained at the animal research facility of the Hebrew University-Hadassah Medical Center. Animals were fed purina (Koffolk 19-520, Koffolk Ltd., Tel Aviv, Israel) and water ad libitum throughout the experiment. All the animals were subjected to bilateral orchietomy (ORX). Six weeks were then allowed to pass prior to implantation. A preliminary study established nearly 40% trabecular bone loss during this time period (Figure 1) with minimal further loss thereafter [5]. At this time, implants with either turned (TU) or sand-blasted-acid-etched (SA) surface were inserted into the proximal metaphysis of one tibia in each animal. The implantation site was analyzed by μ CT and biomechanically 2, 4, 8 and 12 weeks after implant insertion, 9-11 specimens per time point/implant type.

Implantation

We used TU and sand-blasted threaded titanium implants (Dentatus, Hägersten, Sweden; cat. no. TST-S1) (Figures 2A and 2B). The implant shank measures 5 mm in length. Its largest diameter is 0.9 mm tapering to 0.55 mm near the tip. These dimensions allow for convenient and accurate biomechanical testing. SA implants were prepared by further subjecting sand-blasted implants to acid-etching by a commercial implant manufacturer (MIS Implant Technologies, Shlomi, Israel) (Figure 2C).

We have chosen the proximal tibial metaphysis as the implantation site since it is comfortably accessible and composed mainly of trabecular bone. The choice of 13 week old males was because the tibiae of younger or female rats are not large enough to accommodate the entire implant shank. To insert the implant, the antero-medial aspect of the right tibia was exposed at the level of the proximal metaphysis and the insertion path prepared perpendicular to the cortex towards the postero-lateral ridge (Figure 3) using a round low speed dental bur, 0.8 mm in diameter. An attempt was made to prepare the cortical penetration hole 1.5 mm distal to the proximal growth plate which is visible as a line brighter than the bone. The path extended through the cortex and trabecular bone, with the opposite cortex left imperforated. The implant shaft was then threaded into the path leaving 0.5 mm outside the tibia to enable attachment to the biomechanical testing device (Figure 3). The procedure was completed by repositioning the soft tissues and suturing the skin incision. Animals with post-operative swelling or ulceration, malpositioned implants or excessive bone formation around the extracortical part of the implant were excluded from the analysis.

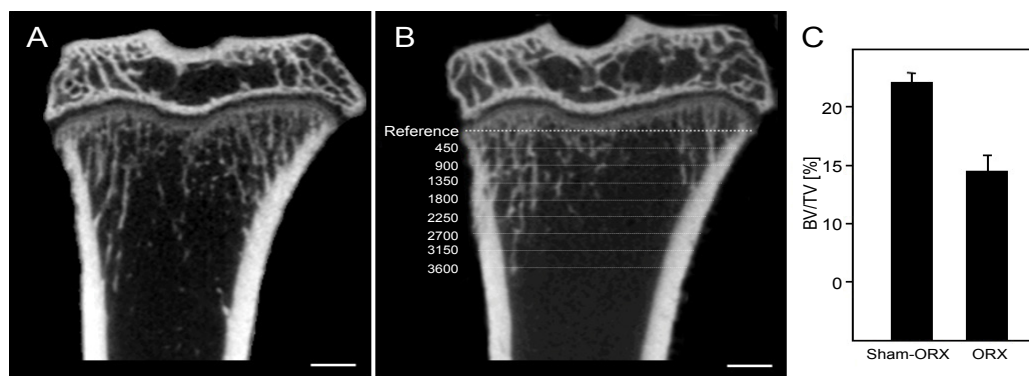


Figure 1: ORX-induced bone loss in proximal tibial metaphysis. (A, B) 2-D μ CT images of frontal plane from representative animals with median trabecular bone volume density (BV/TV) values. (A) Six-week post-operative sham-ORX control. (B) Six-week post-operative ORX rat. Horizontal bold dotted line marks distal-most end of primary spongiosa used as reference line. Non-bolded lines mark segments used to define changes in trabecular bone volume density as function of distance from the reference line (μ m, indicated by numbers). Bars=1 mm. (C) BV/TV. Data are mean \pm SE obtained in 8 rats per condition.

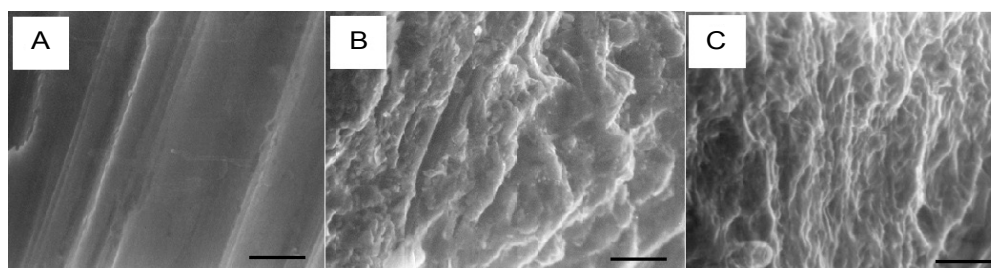


Figure 2: Surface texture of titanium implants. Scanning electron micrographs of (A) TU, (B) Sand-blasted and (C) SA implants. Bars=10 μ m.

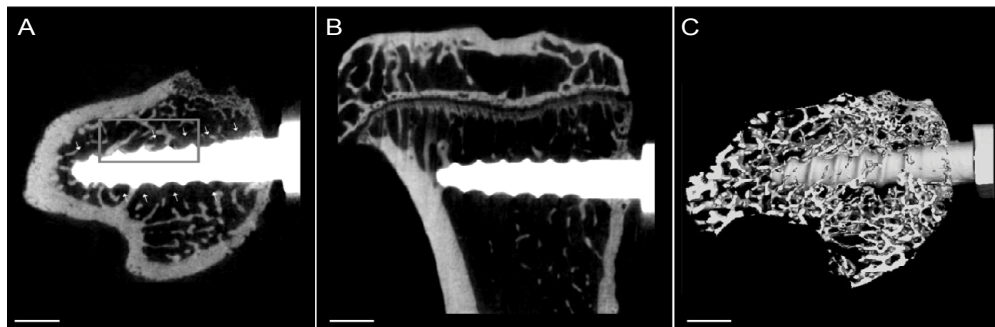


Figure 3: Implant position in secondary spongiosa in proximal tibial metaphysis of ORX rat. (A, B) 2-D μ CT images of through longitudinal axis of SA implant four weeks after insertion. (A) Cross sectional plane; arrows, bright peri-implant halo; box, selected area magnified in Figure 4A. (B) fronto-sagittal plane. (C) 3-D image of same implantation site as in A and B. Bars=1 mm.

Micro-computed tomography

At the time of sacrifice tibiae with implants were separated, transferred for 48 h to phosphate buffered formalin and then kept in 70% ethanol. For a detailed qualitative and quantitative 3D evaluation, the proximal 15 mm of the tibia were examined by a micro-computed tomographic imaging system (μ CT 40, Scanco Medical AG, and Switzerland). For image acquisition, the specimens were mounted on a turntable shifted automatically in an axial direction parallel to the long axis of the implant. The X-ray tube voltage was set to 70 kV, in order to allow maximal X-ray transmission through the highly opaque titanium implant. To maximize signal-to-noise ratio, the system was operated at 114 mA (maximal current for the 70 kV setting) and the longest integration time, 300 msec. Micro-tomographic slices were acquired at 15 μ m slice increment. CT images were reconstructed using a standard convolution-backprojection procedure with a Shepp and Logan filters and was stored in 3-D arrays with an isotropic voxel size of 15 μ m. A constrained 3-D Gaussian filter ($\sigma=1.2$ and support=1) was used to partly suppress the noise in the volumes.

In general, the titanium and mineralized tissue were segmented from each other and from the bone marrow by applying a multi-level thresholding procedure [6,7]. The immediate peri-implant zone could not be segmented together with the rest of the image because it is partially masked by a bright gradient in the attenuation resulting from X-ray artifacts due to the presence of the metallic implant (Figures 3A and 4A). Therefore a new method was devised to also include the 180 μ m wide volume directly affected by the metal artifact surrounding the implant using manufacturer provided scripting software (Image Processing Language, v4.1, Scanco Medical AG, Switzerland) and topological operators (developed internally at the Institute for Biomedical Engineering, ETH and University of Zürich, Switzerland). To this end we defined intervals of the gradient brightness at predetermined distances from the implant (Figure 4A). Segmentation was carried out separately for each interval using specific threshold values. The intervals of the peri-implant zone and the rest of the image were then combined (Figure 4B). Figure 4C demonstrates the combined PIB compartment used for analysis of the following morphometric parameters: bone volume density (BV/TV), trabecular number density (Tb.N) and trabecular thickness (Tb.Th) [8]. To determine the %OI, the ratio between bone and total voxels (Figures 4D and 4E) [9] was calculated in the one voxel thick interval adjacent to the implant (Figure 4A).

Correction for variability in implant positioning

To cater for the inherent variance in implant positioning (a

maximum of ± 1 mm from the target 1.5 mm distal to the primary spongiosa) we used regression formulas that determine the changes in trabecular bone parameters as a function of distance from the primary spongiosa. These formulas were originally calculated in a group of eight rats, six weeks after ORX, according to the exact same methodology as the following animals [10]. In brief, the secondary spongiosa in the proximal tibial metaphysis was divided into 450 μ m thick cross sectional segments covering a zone of 3.6 mm distal to the primary spongiosa (Figure 1B). BV/TV, Tb.N and Tb.Th were determined separately for each consecutive segment. Each of these parameters was then subjected to a curve-fit analysis (SPSS Version 11, SPSS, Chicago, IL, USA), the fit being optimized by the least squares principle [11].

Initial spatial contact between bone and implant is made already at the time of implantation. At this time the visible contacts have no functional significance. However, it is likely that because of their proximity to the implant surface they provide the first sites for genuine osseointegration. Since surgical implant insertion generates a substantial amount of radio opaque debris in contact with the implant (biologically removed shortly after implantation), we assessed the effect of implant positioning on %OI using digital implantation. In this procedure, the 3-D image of a scanned implant was superimposed on the same images used for the curve-fit analysis of the trabecular bone mimicking the actual surgical implantation. Starting at 675 μ m from the primary spongiosa, the implant longitudinal axis was moved distally at 450 μ m increments. The %OI was also subjected to curve-fit analysis, covering the same trabecular bone compartment as above.

The resulting prediction curves for each morphometric parameter, as previously published [10], were used to correct the observed measurement, based on the actual distance of the implant from the 1.5 mm target distance.

Biomechanical testing

Following μ CT analysis, the implants were subjected to pullout testing. The bony and implant parts of each specimen were firmly connected to a commercial material testing system (Zwick, Ulm, Germany). For near linear displacement we used a jig designed specifically for the present model whereby ball joints were employed to connect the fixtures (Figure 5). Tests were performed using a displacement rate of 1 mm/min. Stiffness, ultimate force and toughness were determined for the bone-implant system from the resulting load-displacement curves.

Statistical comparisons

All comparisons were analyzed using SigmaStat software (SPSS,

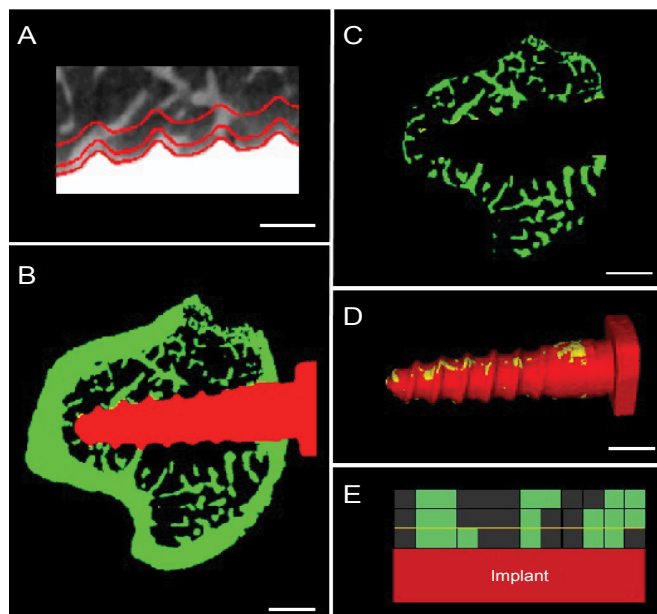


Figure 4: μ CT quantification of %OI and PIB parameters. (A) High magnification of boxed area in Figure 3A showing X-ray peri-implant halo. Red lines indicate intervals used for stepwise segmentation as function of distance from implant surface. First, second and third lines delimit 15, 60 and 105 μ m intervals, respectively, of decreasing scattering-induced "brightening" segmented using decreasing threshold values. (B) Same 2-D slices as in Figure 3A showing differential segmentation of implant (red) and bone (green). (C) 2-D image of PIB extracted from B. (D) 3-D segmented image of implantation site shown in Figure 3. Yellow patches indicate implant surface in contact with trabecular bone. (E) schematic demonstration of automatic calculation of %OI as ratio between number of "bone" (green) and total voxels in contact with implant (delimited by yellow line); dark voxels represent radiolucent tissue.

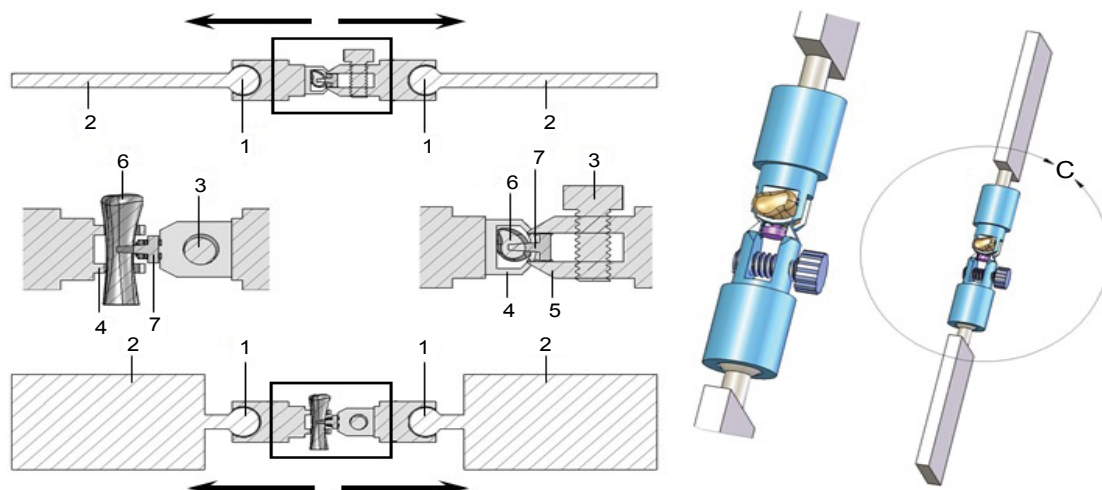


Figure 5: Drawings of jig for pullout testing. Top, proxo-distal view of tibia; inset, enlarged part shown in right middle. Bottom, antero-posterior view of tibia; inset, enlarged part shown in left middle. Right, 3D schematic representation of the jig and bone sample. Arrows, pull force vector; (1) ball joint; (2) plate for attachment to testing system; (3) tightening screw; (4) ring fixture for tibia; (5) tweezers fixture for implant; (6) proximal tibia; (7) implant.

Chicago, IL, USA). Differences in quantitative μ CT and biomechanical parameters among time/implant surface texture groups were tested by analysis of variance (2-way ANOVA). When significant differences were indicated by ANOVA, means of pairs of groups were compared using the Student-Newman-Keuls method for multiple comparisons. Pearson correlation coefficients were calculated to assess the relationship between mechanical and quantitative μ CT measurements.

Results

Using settings of the μ CT apparatus that result in enhanced X-ray

transmission through the titanium implant, we were able to generate 2- and 3-D images that clearly depict the bone-implant interface, thus identifying bone in close contact with the implant (Figures 3 and 4).

Six weeks post ORX the metaphyseal trabecular bone reaches a new steady state whereby further decreases in the quantitative structural parameters are minimal [5]. Therefore, the present curve-fit analysis of quantitative μ CT parameters, aimed at providing a method for correcting the positional errors occurring at the time of implantation, was performed in the proximal tibial metaphysis at the six week time

point. This analysis demonstrates decreasing logarithmic gradients of the BV/TV and Tb.N from the primary spongiosa distally (Figures 6A-6C). The resulting regression curves show excellent fitness between the observed and predicted values with very high percent explained variation ($r^2=0.894$ and 0.840 for BV/TV and Tb.N, respectively). Logarithmic gradients with very high fitness for these parameters were also found in normal male rats of the same age (data not shown). No such trend is evident for Tb.Th, which shows similar values within the entire metaphyseal compartment (108 ± 1.9 and $77 \pm 0.8 \mu\text{m}$ in normal and ORX rats, respectively). In addition, the Tb.Th curves show rather poor fitness between observed and predicted values ($r^2=0.293$) (Figure 6C). Therefore, Tb.Th was not corrected in further analyses. The %OI values for the digital "implantation" on distance from the primary spongiosa also show a logarithmic regression curve with $r^2=0.826$ (Figure 6D). The following equation was used to correct for positional variation:

$$P_c = P_m - \kappa [\ln(D_c) - \ln(D_m)]$$

Where P_c is the corrected value for a pre-determined arbitrary distance from the distal tip of the primary spongiosa D_c ($1,500 \mu\text{m}$ in the present analysis), P_m represents the measured value at an actual distance D_m , κ is the parameter-specific slope of the fitness regression equations (Figures 6A-6D).

The osseous reaction to implantation is shown in Figure 6. All the corrected PIB parameters decrease between weeks 2 and 8 after implantation. This decrease is significant for the BV/TV and Tb.N and not significant for the Tb.Th. Thereafter, these parameters stabilize at the pre-implantation level. This trend is the consequence of an initial post-implantation increase in BV/TV and Tb.N (Figures 7A and 7B). Notably, the Tb.Th is significantly higher than pre-implantation level throughout the 12 week follow up period (Figure 7C). Differences between the PIB changes in response to the two types of implant are subtle and did not reach statistical significance (Figure 7). The %OI

shows an opposite trend, namely, a roughly linear, 150% increase 2-12 weeks after implantation (Figure 7D). Unlike the PIB parameters, the %OI of TU implants is significantly higher compared to SA implants at all-time points except week 8. Apparently, this difference resulted from an initial modulation of bone formation in contact with the implant immediately after implantation, inasmuch as it remained approximately the same (other than the 8 week time point) thereafter (Figure 7D). At the time of implantation, several trabeculae make apparent contact with the implant surface (Figure 6D). However, this apparent contact cannot be attributed to functional osseointegration but to close proximity between the cut edges of pre-existing trabeculae and the implant surface. The continuous increase in %OI over the alleged %OI calculated at the time of implantation (Figure 6D) is evident already on week 2 after implantation and suggests continuous *de novo* bone formation induce by, and in contact with, the implant surface.

Because a curve-fit analysis for the biomechanical parameters, which is based on pre-implantation values, is not attainable, the present statistical analysis of these parameters employed measurements that were not corrected for positional variability. Still, in the case of TU implants, all the biomechanical parameters show 2- to 3-fold increase during the 12 week follow-up period (Figure 8), which becomes statistically significant eight weeks after implantation and with the values remaining at similar high levels a month later. Although the general trend of progressive improvement in mechanical properties is also shared by the SA implants (Figure 8), increases for these implants failed to gain statistical significance except the ultimate force after twelve weeks (Figure 8B). At weeks 8 and 12 all the biomechanical parameters show higher values for TU over SA implant surface. However, this difference is not statistically significant (Figure 8).

The correlation analysis between uncorrected quantitative μCT and biomechanical parameters revealed significant correlation coefficients only between the latter and %OI (Table 1). The strongest relationship

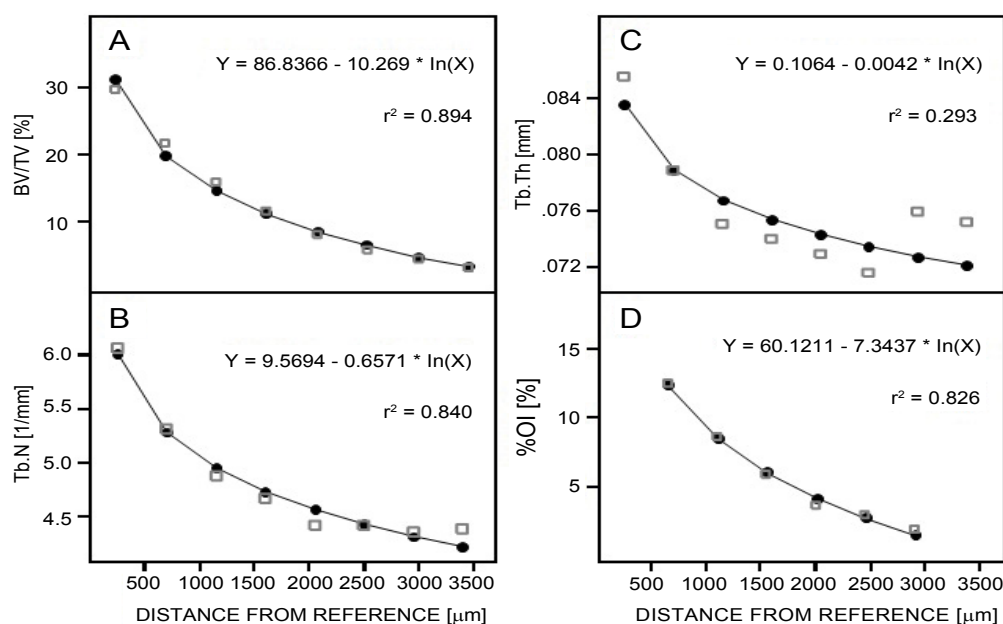


Figure 6: Curve fit analysis 6 weeks post-ORX demonstrating changes in metaphyseal trabecular bone parameters and %OI as function of distance from distal end of proximal tibial primary spongiosa. Abscissa is distance of layers defined in Figure 2B. Ordinate is value calculated in corresponding layers. (A) trabecular volume density (BV/TV); (B) trabecular number density (Tb.N); (C) trabecular thickness (Tb.Th); (D) %OI. ●, predicted values; □, observed values; r^2 =percent explained variation between observed and predicted value.

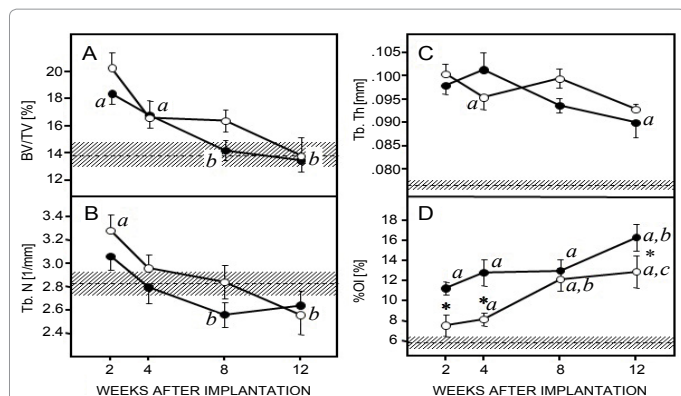


Figure 7: Temporal changes in PIB parameters and %OI following insertion of TU and SA implants into proximal tibial metaphysis of ORX rats. (A) Trabecular bone volume density (BV/TV); (B) Trabecular number density (Tb.N); (C) Trabecular thickness (Tb.Th); (D) %OI. ●, TU implants; ○, SA implants. Data are mean ± SE obtained in 8-11 animals per condition; a, Mann-Whitney U-test, $p < 0.05$; (b, c) ANOVA. b, labeled time point vs. 2W; c, labeled time point vs. 4W, $p < 0.05$. *, ANOVA, ● vs. ○, $p < 0.05$. Dashed line, immediate pre-implantation level (striekthrough zone represents SE).

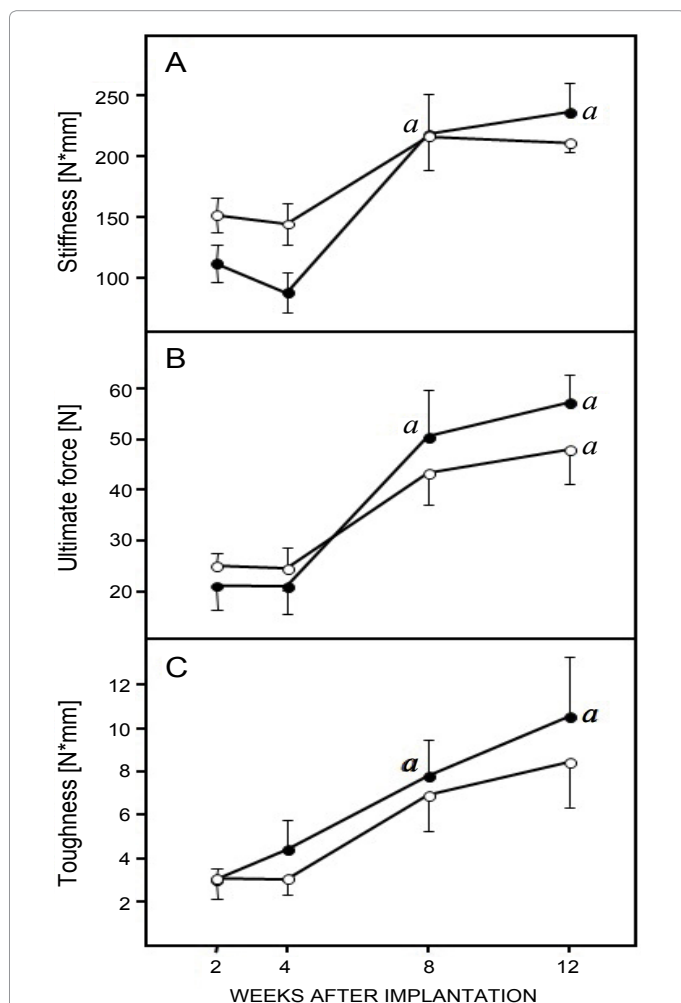


Figure 8: Temporal changes in biomechanical parameters following insertion of TU and SA implants into proximal tibial metaphysis of ORX rats. (A) Stiffness; (B) Ultimate force; (C) Toughness. ●, TU implants. ○, SA implants. Data are mean ± SE obtained in 6-9 animals per condition. a, ANOVA, labeled time point vs. 2W, $p < 0.05$.

is with the ultimate force, highlighting the critical importance of the amount of bone-implant contact.

Discussion

The present study demonstrates the advantages of the μ CT analysis over histomorphometry and scanning electron microscopy. With all voxels in the reference volume included in the analysis, it is free of sampling errors resulting from the selection of suboptimally representative planes and from the unavoidable inter-specimen variation in plane orientation relative to the implant and skeletal landmarks. Combining the statistical high resolution with the technical high resolution of the μ CT apparatus and implant positional correction we were able to show statistically significant temporal trends over a prolonged post-implantation period (12 weeks) and reveal the effect of implant surface texture on the amount of bone in contact with the implant, but not on the PIB. Last but not least, the non-destructive nature of the μ CT analysis facilitated biomechanical testing of the same specimens and the consequent demonstration of correlation between the morphometric and biomechanical measurements.

The most popular endosseous implantation models in rodents are the intramedullary nailing with cylindrical rods [12,13] and intrametaphyseal insertion of tapered, threaded implants [14,15]. In the intramedullary nail model, significant segments of the implant are embedded in both metaphyseal trabecular bone and diaphyseal bone marrow (and later the bone marrow derived reactive bone). By contrast, the intrametaphyseal model is biologically more homogenous in the sense that other than a small cylindrical segment of the implant in contact with cortical bone, the entire threaded part is surrounded uniformly by trabecular bone. Still, a handful of studies in rats show images with substantial variation within the metaphyseal trabecular network, namely a progressive decrease in trabecular bone volume density as a function of distance from the growth plate. Our pre-implantation quantitative μ CT analysis in normal and osteopenic rats confirms this common observation and assigns a mathematical function to this gradient (gabet) [10]. We further used this function for correcting the unavoidable variation in implant positioning. Prior to correction, the standard error of our measurements was 20-30% of the mean (data not shown), a variation typically reported in implantation experiments using the rat proximal tibial metaphysis [14-17]. The corrected standard errors were around or below 10%, suggesting that variations in implant positioning account for a substantial decrease in the signal-to-noise ratio. Perhaps more importantly, the correction enhanced the power of our statistical analysis, resulting in the demonstration of a significant difference in %OI between implants with distinct surface textures. Importantly, the curve-fit analysis aimed at defining the mathematical formula has to be performed using the exact same settings as for the implantation model. The formulas are likely to differ according to the animal model (species, strain, sex, age...), as well as μ CT apparatus and settings.

Accurately determining the %OI at high resolution is a challenging task. A comprehensive review on the different protocols for μ CT analysis of the %OI around metallic implants concluded that using only one threshold value for image segmentation, accurate measurement are unattainable [18]. To avoid false positive %OI measurements resulting

	Stiffness	Ultimate force	Toughness
%OI	$r=0.300$ $p=0.021$	$r=0.419$ $p<0.001$	$r=0.357$ $p=0.005$

Table 1: Correlation coefficients between μ CT morphometric and biomechanical properties of the implant-bone complex.

from the peri-implant X-ray scattering artifacts, previous μ CT analyses of implant anchorage either applied a subjective identification of bone-implant contacts in 2-D images [13] or allowed for a 45 μ m gap in the immediate vicinity of the implant that could not be analyzed [9]. By contrast, the present automatic determination using multilevel thresholding reduced the X-ray metal artifacts, thus allowing the determination of the bone-implant contact at the 15 μ m voxel resolution. In addition, the multilevel thresholding enabled inclusion of the immediate implant vicinity in the PIB compartment.

The present and previous [13] results demonstrate opposite post-implantation trends in the %OI vs. PIB parameters. The %OI increases progressively with time after implantation, apparently consequent to induction of osteoblast activity by the titanium implant [19]. The initial elevation in PIB parameters during the first couple of weeks after implantation is attributable to the osteogenic bone marrow reaction to the injury associated with implant insertion [20]. This reaction consists of *de novo* primary bone formation in the inter-trabecular spaces and increased bone formation on the surfaces of pre-existing trabeculae. The decrease in these parameters that follows results from remodeling of the reactive bone [20].

Both, the %OI and biomechanical parameters showed progressive temporal increase during the experimental follow up period. In addition, both showed higher values for the TU implants. That the differences in biomechanical parameters were not statistically significant may have resulted, at least in part, from the greater variability inherent in the assay system and due to the lack of positional correction for these measurements. Intuitively, a correlation between the biomechanical and morphometric PIB parameters is expected inasmuch as the PIB connects the implant with the surrounding cortex. We therefore assume that a genuine correlation does exist that is masked by the active PIB remodeling. Demonstrating this correlation probably requires a longer post-implantation follow up period.

The power of using μ CT for the analysis of implant anchorage in trabecular bone is shown here by (i) the specific correlation between the %OI and biomechanical parameters; (ii) the discrimination between two implant types. Furthermore, we demonstrate the applicability of the rat tibial metaphyseal model for testing the effect of modifications to the implant surface and for studying the mechanisms involved in implant anchorage in the context of low density trabecular bone.

Acknowledgement

Purchase of the μ CT system by the Bone Laboratory was supported in part by ISF grant to IB (9007/01). RM was supported through the SNF Professorship in Bioengineering of the Swiss National Science Foundation (FP 620-58097.99 and PP-104317/1).

Manufacturers

Purina: Koffolk 19-520, Koffolk Ltd., Tel Aviv, Israel

Implants: Dentatus; cat. no. TST-S1

Chemical etching of implants performed by MIS Implant Technologies, Shlomi, Israel

μ CT 40: Scanco Medical

Image Processing Language, Version 4.1: Scanco Medical

SPSS Version 11: SPSS

SigmaStat software: SPSS

Material testing system: Zwick.

References

1. Kaneko S, Tsuru K, Hayakawa S, Takemoto S, Ohtsuki C, et al. (2001) *In vivo* evaluation of bone-bonding of titanium metal chemically treated with a hydrogen peroxide solution containing tantalum chloride. *Biomaterials* 22: 875-881.
2. Oosterbos CJ, Vogely HCh, Nijhof MW, Fleer A, Verbout AJ, et al. (2002) Osseointegration of hydroxyapatite-coated and non-coated Ti6Al4V implants in the presence of local infection: A comparative histomorphometrical study in rabbits. *J Biomed Mater Res* 60: 339-347.
3. Bauer TW, Schils J (1999) The pathology of total joint arthroplasty. I. Mechanisms of implant fixation. *Skeletal Radiol* 28: 423-432.
4. Meraw SJ, Reeve CM (1999) Qualitative analysis of peripheral peri-implant bone and influence of alendronate sodium on early bone regeneration. *J Periodontol* 70: 1228-1233.
5. Gabet Y, Kohavi D, Muller R, Chorev M, Bab I (2005) Intermittently administered parathyroid hormone 1-34 reverses bone loss and structural impairment in orchietomized adult rats. *Osteoporos Int* 16: 1436-1443.
6. Muller R, Ruegsegger P (1997) Micro-tomographic imaging for the non-destructive evaluation of trabecular bone architecture. *Stud Health Technol Inform*. 40: 61-79.
7. Ruegsegger P, Koller B, Muller R (1996) A microtomographic system for the non-destructive evaluation of bone architecture. *Calcif Tissue Int* 58: 24-29.
8. Alexander JM, Bab I, Fish S, Müller R, Uchiyama T, et al. (2001) Human parathyroid hormone 1-34 reverses bone loss in ovariectomized mice. *J Bone Miner Res* 16: 1665-1673.
9. Rebaudi A, Koller B, Laib A, Trisi P (2004) Microcomputed tomographic analysis of the peri-implant bone. *Int J Periodontics Restorative Dent* 24: 316-325.
10. Gabet Y, Kohavi D, Kohler T, Baras M, Muller R, et al. (2008) Trabecular bone gradient in rat long bone metaphyses: Mathematical modeling and application to morphometric measurements and correction of implant positioning. *Journal of Bone and Mineral Research: The Official Journal of the American Society for Bone and Mineral Research* 23: 48-57.
11. Woolson R (1987) *Statistical methods for the analysis of biomedical data*. John Wiley and sons, New York, USA.
12. Braun G, Kohavi D, Amir D, Luna M, Caloss R, et al. (1995) Markers of primary mineralization is correlated with bone-bonding ability of titanium or stainless steel *in vivo*. *Clin Oral Implants Res* 6: 1-13.
13. Kuroda S, Viridi AS, Li P, Healy KE, Sumner DR (2004) A low-temperature biomimetic calcium phosphate surface enhances early implant fixation in a rat model. *J Biomed Mater Res A* 70: 66-73.
14. Shiota T, Tashiro M, Ohno K, Yamaguchi A (2003) Effect of intermittent parathyroid hormone (1-34) treatment on the bone response after placement of titanium implants into the tibia of ovariectomized rats. *J Oral Maxillofac Surg* 61: 471-480.
15. Yamazaki M, Shiota T, Tokugawa Y, Motohashi M, Ohno K, et al. (1999) Bone reactions to titanium screw implants in ovariectomized animals. *Oral Surg Oral Med Oral Pathol Oral Radiol Endod* 87: 411-418.
16. Okamura A, Ayukawa Y, Iyama S, Koyano K (2004) Effect of the difference of bone turnover on peri-titanium implant osteogenesis in ovariectomized rats. *J Biomed Mater Res A* 70: 497-505.
17. Tokugawa Y, Shiota T, Ohno K, Yamaguchi A (2003) Effects of bisphosphonate on bone reaction after placement of titanium implants in tibiae of ovariectomized rats. *Int J Oral Maxillofac Implants* 18: 66-74.
18. Liu S, Broucek J, Viridi AS, Sumner DR (2012) Limitations of using micro-computed tomography to predict bone-implant contact and mechanical fixation. *J Microsc* 245: 34-42.
19. Beloti MM, Bellesini LS, Rosa AL (2005) The effect of purmorphamine on osteoblast phenotype expression of human bone marrow mesenchymal cells cultured on titanium. *Biomaterials* 26: 4245-4248.
20. Bab IA, Einhorn TA (1994) Polypeptide factors regulating osteogenesis and bone marrow repair. *J Cell Biochem* 55: 358-365.